PAPER

Advantages and disadvantages of vacuum-deposited and spin-coated amorphous organic semiconductor films for organic light-emitting diodes†

Maki Shibata,[a] Yoshiya Sakai[b] and Daisuke Yokoyama*[abc]

To realize low-cost fabrication processes for high-performance organic light-emitting diode (OLED) display and lighting, it has recently become important to understand the properties and structures of solution-processed amorphous films. In particular, to choose an appropriate process to produce OLEDs to meet the demands of a realistic situation, it is necessary to know the general advantages and disadvantages of vacuum- and solution-processed films quantitatively. However, the differences between the films formed by these processes are not yet sufficiently clear. Here we systematically compare vacuum-deposited and spin-coated amorphous organic semiconductor films used for OLEDs mainly by ellipsometry, and demonstrate the critical differences in film density, transition temperature, and molecular orientation. We found that the film density, transition temperature, and degree of horizontal molecular orientation of small-molecule spin-coated films are inherently lower than those of the corresponding vacuum-deposited ones. In addition, we show that the transition temperature and molecular orientation of small-molecule spin-coated films of glassy materials are identical to those of "deteriorated" vacuum-deposited films that have experienced a transition induced by heating. Our comprehensive comparisons lead to guidelines for selecting suitable processes and materials for production and clarify the future challenges to be addressed to facilitate the development of high-performance solution-processed OLEDs.

1. Introduction

Research on organic light-emitting diodes (OLEDs), which are promising optoelectronic devices for display and lighting, has grown continuously with the development of amorphous organic semiconductor materials. Since the first report of OLEDs using thin films,[1] amorphous organic films have been used in most OLEDs mainly because of their smooth surface, which ensures the high uniformity and stability of devices under a high electric field. As the performance of OLEDs has been improved to a high level to allow wide commercialization, it has become important to obtain a much deeper understanding of the higher-order structures in the amorphous films to control

and further improve OLED performance,[2] even though the randomness in amorphous films makes this task difficult.

Amorphous films for OLEDs can be roughly categorized into two groups depending on their fabrication process: vacuum-processed films, and solution-processed films. In addition, solution-processed films can be further divided into two groups with respect to their molecular size: small-molecule solution-processed films, and polymer solution-processed films. Most commercialized OLEDs are currently based on vacuum-processed films, because they enable us to easily fabricate ideal multilayer structures with very high purity. Meanwhile, the use of solution-processed films has recently drawn increasing attention to realize low-cost fabrication of large-area printable OLEDs with high performance.[3] The films in the above three categories have advantages and disadvantages when compared to each other. Thus, when we choose an appropriate process and materials to produce OLED displays or lighting to meet the demands of a realistic situation, it is very important to quantitatively understand the general advantages and disadvantages of these films.

However, the differences between small-molecule vacuum- and solution-processed films, and also between small-molecule and polymer solution-processed films, have not been systematically discussed from the viewpoint of the higher-order structures of the molecules in the amorphous films. Although the differences

[a] *Department of Organic Device Engineering, Yamagata University, 4-3-16 Jonan, Yonezawa, Yamagata 992-8510, Japan. E-mail: d_yokoyama@yz.yamagata-u.ac.jp; Fax: +81-238-26-3890; Tel: +81-238-26-3890*

[b] *Department of Polymer Science and Engineering, Yamagata University, 4-3-16 Jonan, Yonezawa, Yamagata 992-8510, Japan*

[c] *Research Center for Organic Electronics (ROEL), Yamagata University, 4-3-16 Jonan, Yonezawa, Yamagata 992-8510, Japan*

† Electronic supplementary information (ESI) available: UV-vis absorption, XRR, ellipsometry, XRD, and surface morphology results for sample films, along with experimental conditions for sample fabrication. See DOI: 10.1039/c5tc01911g

11178 | *J. Mater. Chem. C,* 2015, **3**, 11178–11191

This journal is © The Royal Society of Chemistry 2015

between small-molecule vacuum- and solution-processed films of some OLED materials have been reported,[4–9] they were mainly for a single material or device, and fundamental discussion of the differences based on comprehensive investigation has not been carried out sufficiently. In addition, in some cases, wrong conclusions have been drawn, probably because of poor accuracy of analysis or misinterpretation of the experimental results.

To consider the differences between small-molecule vacuum- and solution-processed films, the recent studies on vacuum-processed films reported by Ediger and co-workers are very informative. They reported a relatively high density and specific stability of vacuum-deposited glasses of some organic materials compared with those of the corresponding ordinary glasses commonly formed from supercooled liquids.[10–14] Ishii and co-workers also investigated the specific behaviour of vacuum-deposited organic glasses and discussed their densities.[15,16] The reports by these groups show the distinguished nature of vacuum-processed films, which inspired us to investigate the critical differences between vacuum- and solution-processed films.

In this study, we systematically investigate the differences between the physical properties of small-molecule vacuum-deposited and spin-coated films used for OLEDs by ellipsometry, ultraviolet-visible (UV-vis) absorption and X-ray reflectivity (XRR) measurements. In particular, we focus on the differences in the three factors of the films: (i) film density (with absolute values), (ii) transition temperature, and (iii) molecular orientation. As shown in Fig. 1, these factors are important to discuss the characteristics of devices, because (i) the film density affects the overlap of molecular orbitals, which can affect charge transport and energy transfer between two adjacent molecules; (ii) the transition temperature is directly related to the thermal durability of films and devices;[17] and (iii) the molecular orientation strongly affects both the electrical and optical characteristics of devices.[2] We found that the film density, transition temperature, and degree of horizontal molecular orientation of small-molecule spin-coated films are inherently lower than those of vacuum-deposited films. We also show that the molecular orientation and transition temperature of small-molecule spin-coated films of glassy materials are identical to those of the "deteriorated" vacuum-deposited films that have experienced a transition induced by heating. In addition, we compare the transition

temperatures and molecular orientations of small-molecule and polymer spin-coated films with similar molecular units and confirm that the transition temperature and degree of horizontal molecular orientation of the former are lower than those of the latter. Our results reveal some general disadvantages of the higher-order structures in small-molecule spin-coated films at present and lead to guidelines for choosing a process or materials for device production. Our systematic comparisons and related discussions also clarify the future challenges to be addressed to facilitate the development of high-performance solution-processed OLEDs.

2. Results and discussion

2.1 Film density

We used three methods to accurately determine the absolute densities of vacuum-deposited and spin-coated films. The first was UV-vis absorption measurements of solutions of dissolved films.[18,19] From the absorbance of a solution of a dissolved film with a definite film volume, we determined the absolute density averaged in the overall film by comparison with the absorbance of reference solutions. The second method was XRR measurement.[20] From the critical angle for an organic film on a substrate obtained from its XRR pattern, we determined the absolute density at the film surface (to a depth of a few nanometers).[21,22] These two methods can determine the absolute density of films, but are not suitable for all films; they both need a highly uniform film with a large area, and are time-consuming when there are many samples. In UV-vis absorption measurements, it is necessary to prepare sample films with high uniformity over a large area to precisely define the film volume. In addition, the dissolved solution and reference solutions need to be prepared very carefully to minimize concentration errors. XRR measurements also require uniform sample films with a large area. Because the critical angle for organic films in XRR patterns is generally very small, uniform large films are needed to sufficiently shine the X-rays with such a small grazing incident angle onto the sample film. Thus, these two methods were too difficult to apply to the numerous sample films (>100) in this study, especially to the spin-coated films, which are not as uniform as the vacuum-deposited ones.

The third method is ellipsometry, which enables us to analyze films quickly, and only needs a small uniform area of a few millimeters square. However, ellipsometry can only determine relative densities. From the refractive index of a film in the transparent spectral region, relative densities can be determined using the Lorentz–Lorenz equation (see Section 4.4 for details). By combining the relative densities of all films of a material determined by ellipsometry with the absolute densities of a few films of the material determined by UV-vis absorption and XRR measurements, we can determine the absolute densities of all films of the material.

To compare the densities of vacuum-deposited and spin-coated films, we first used four common OLED materials shown on the left side of Fig. 2: 4,4′-bis[N-(p-tolyl)-N-phenylamino]biphenyl (TPD), 4,4′-bis[N-(1-naphthyl)-N-phenylamino]biphenyl (α-NPD),
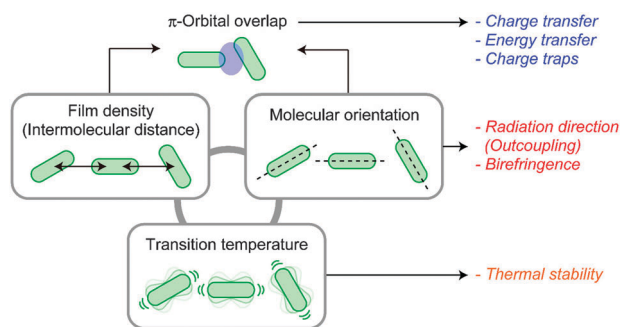

Fig. 1 Schematic diagram outlining the importance of the film density, molecular orientation, and transition temperature of amorphous organic semiconductor films in OLEDs.
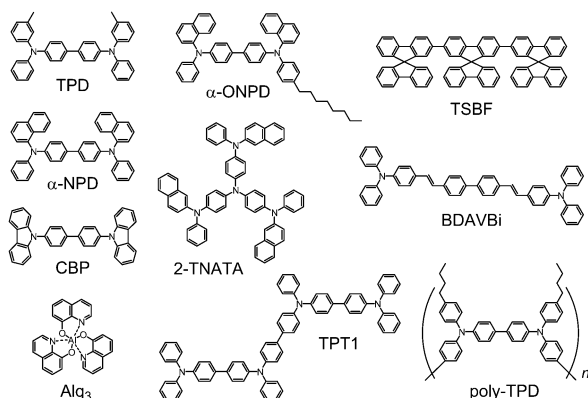
This journal is © The Royal Society of Chemistry 2015

J. Mater. Chem. C, 2015, 3, 11178–11191 | 11179

Fig. 2 Amorphous OLED materials used in this study.

4,4′-bis(N-carbazole)biphenyl (CBP), and tris(8-hydroxyquinoline)-aluminum (Alq$_3$). We selected these materials for the analysis of density, because their birefringences in the transparent spectral region are small[23,24] enough to simplify the XRR and ellipsometry analyses using isotropic optical models. Fig. 3(a) shows the average densities of the vacuum-deposited TPD films obtained from UV-vis absorption measurements of solutions of dissolved films with thicknesses of ∼50, 100, 150, and 200 nm (see Fig. S1(a), ESI† for more details). The average density of vacuum-deposited TPD

films with a thickness of >50 nm was 1.14 ± 0.02 g cm^{-3}. Meanwhile, the density at the surface of a vacuum-deposited TPD film with a thickness of 330 nm on a Si(100) substrate was determined by XRR measurements (Fig. 3(b)). Fitting analysis using theoretical curves indicated that the density at the surface was 1.18 ± 0.04 g cm^{-3}, which is slightly higher than the average density, though the difference is within the error. Table 1 summarizes the average and surface densities of vacuum-deposited films of each material (detailed data are provided in Fig. S1(a)–(d) and S2, ESI†). For all of the four materials, the surface densities of vacuum-deposited films (values in parentheses) are slightly higher than their average densities. We think that this is related to the time for surface diffusion of molecules. Molecules buried in the bulk of a film do not have much time for surface diffusion enough to find a sufficiently stable state as those on the surface because of the deposition of successive molecules overlaying onto them. However, we can assume that this high-density region at the film surface is not thick because the average densities for the overall films do not decrease apparently with increasing film thickness. Thus, hereafter we will mainly discuss the average densities determined from UV-vis absorption measurements of the solutions of dissolved films. These values can be directly associated with the relative densities determined by ellipsometry measurements, which are optically averaged in overall films.

Compared to the densities of the vacuum-deposited films, those of the corresponding spin-coated films were lower for all four materials. Fig. 4 shows the thicknesses and densities of spin-coated TPD films fabricated on Si(100) substrates using chloroform as the solvent with different spin speeds and solution concentrations. The absolute values of the densities of the spin-coated films were relatively determined from those of the vacuum-deposited films and the differences between the relative densities of vacuum-deposited and spin-coated films. In general, the slower the spin speed is and also the higher the solution concentration is, the thicker the spin-coated film becomes. The densities of the spin-coated films converged to a value of 1.12 ± 0.02 g cm^{-3}, which is lower than that of the vacuum-deposited films, when the film thickness exceeded 18 nm. The densities of very thin (<10 nm) films were seemingly much lower than this value because such thin films are not uniform on Si substrates, so the values are a mixture of the densities of the material and air. We also performed the same experiments for the other three materials, resulting in
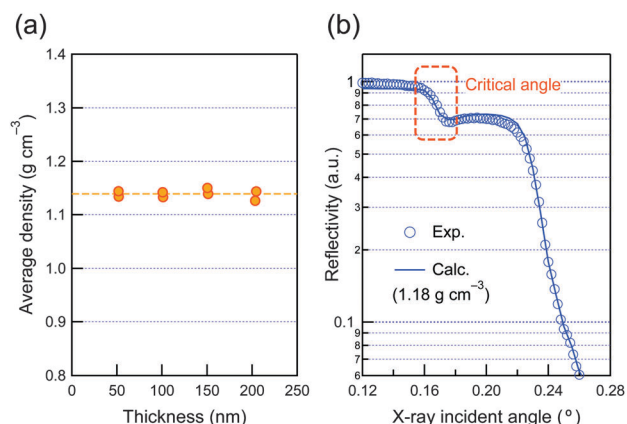

Fig. 3 (a) Densities averaged in the overall thickness of vacuum-deposited TPD films determined by absorption measurements of solutions of the dissolved films. (b) XRR pattern of a vacuum-deposited TPD film with a thickness of 330 nm on a Si(100) substrate. The theoretical curve for a density of 1.18 g cm^{-3} is also shown.

Table 1 Absolute densities and packing coefficient K_p of single crystals, vacuum-deposited films, and spin-coated films of the materials

	Materials	TPD	α-NPD	CBP	Alq$_3$	α-ONPD	2-TNATA	TPT1	TSBF	BDAVBi
Density[a]	Single crystal[b]	1.21	—	1.31	1.42	—	—	—	—	—
	Vacuum-deposited[c]	1.14 (1.18)	1.17 (1.19)	1.17 (1.21)	1.30 (1.34)	1.16	1.17	1.15	1.16	1.18
	Spin-coated	1.12	1.14	1.13	1.28	1.15	1.15	1.13	1.14	1.17
K_p	Single crystal[b]	0.68	—	0.70	0.69	—	—	—	—	—
	Vacuum-deposited	0.66	0.67	0.65	0.66	0.69	0.66	0.65	0.64	0.68
	Spin-coated	0.65	0.65	0.63	0.65	0.68	0.65	0.64	0.63	0.68

[a] The unit of all densities is g cm^{-3}. [b] The values were obtained using the crystallographic data in ref. 25–27. [c] The values in parentheses are densities at the film surface determined by XRR measurements.

11180 | J. Mater. Chem. C, 2015, 3, 11178–11191

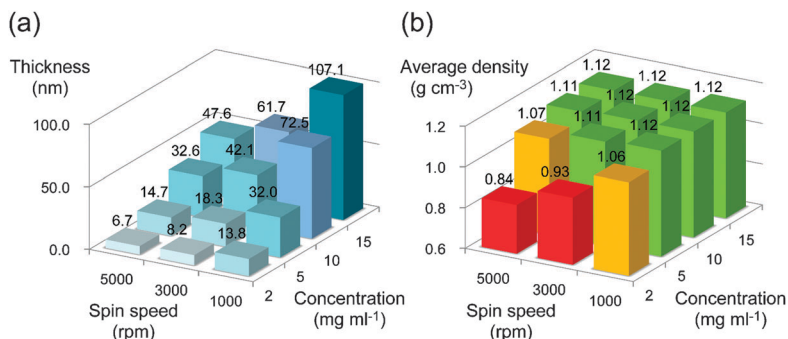This journal is © The Royal Society of Chemistry 2015

Fig. 4 (a) Thicknesses and (b) film densities of spin-coated TPD films fabricated using chloroform as the solvent with different spin speeds and solution concentrations.

qualitatively similar trends (see Fig. S3(a)–(c), ESI†). The absolute densities of the spin-coated films fabricated using chloroform are also summarized in Table 1. The densities of the spin-coated films of all these materials were lower than those of the vacuum-deposited films.

To investigate the dependence of the film density on the solvent, we further determined the densities of spin-coated TPD films fabricated using other many kinds of solvents having different boiling points: 1,4-dioxane (101 °C), toluene (111 °C), butylacetate (126 °C), cyclopentanone (131 °C), chlorobenzene (132 °C) and o-dichlorobenzene (180 °C), which all have boiling points that are higher than that of chloroform (61 °C). Because the boiling point of a solvent affects how quickly the solvent is vaporized during the spin-coating process, we considered the possibility that the solvent might also affect the density of films. However, as shown in Fig. 5, the densities of the films fabricated using these solvents were almost the same as those of the films fabricated using chloroform when the film thickness was >30 nm (see Fig. S4, ESI† for more details). This suggests that the dependence of the densities of spin-coated films on the solvent is small, and that spin-coated films generally have lower densities than vacuum-deposited ones. In addition to the densities of the films, Table 1 also shows the

densities of single crystals of three materials, which were calculated from the crystallographic data.[25–27] From these results, we conclude that the densities of the solids of small-molecule amorphous OLED materials have the order of single crystal > vacuum-deposited film > spin-coated film.

We also estimated the packing coefficient K_p,[28] which represents how densely molecules are packed in each solid, using the densities obtained above and the following equation:

$$K_p = \frac{V_{vdW}}{V_m} = \frac{\rho N_A V_{vdW}}{M}, \tag{1}$$

where V_{vdW} is van der Waals volume of a molecule,[29] V_m is molecular volume (the volume per molecule), ρ is density of the solid, N_A is the Avogadro constant, and M is molecular weight. The value of $1 - K_p$ indicates the void in the solid. Here the values of V_{vdW} in vacuum-deposited and spin-coated films were estimated using the optimized molecular structures obtained by density functional theory (DFT) B3LYP/6-31G(d) calculations.[30] The results are summarized in Table 1, showing that the packing coefficients of vacuum-deposited and spin-coated amorphous films are not highly dependent on materials.

The absorption spectra of solid films on fused silica substrates also show definite differences between vacuum-deposited and spin-coated films. Fig. 6 shows the UV-vis absorption spectra of vacuum-deposited and spin-coated TPD films on fused silica substrates. To accurately and fairly compare the spectra, we fabricated sample films with approximately the same thickness of 53 ± 4 nm. We used the similar thickness to unify the interference effect on spectra in absorption measurements using a spectrophotometer, which can substantially change the spectral shape (see Fig. S5, ESI†). The absorption spectra of the four spin-coated films fabricated using different four solvents were the same, but differed from that of the vacuum-deposited film. The difference between the absorption spectra of the vacuum-deposited and spin-coated films would originate from slight differences in molecular orientation and the overlap of electronic orbitals of adjacent molecules. A similar difference was also observed for α-NPD (see Fig. S6, ESI†). The fact that the absorption spectra of the spin-coated films are independent of the solvent suggests that they are macroscopically identical.
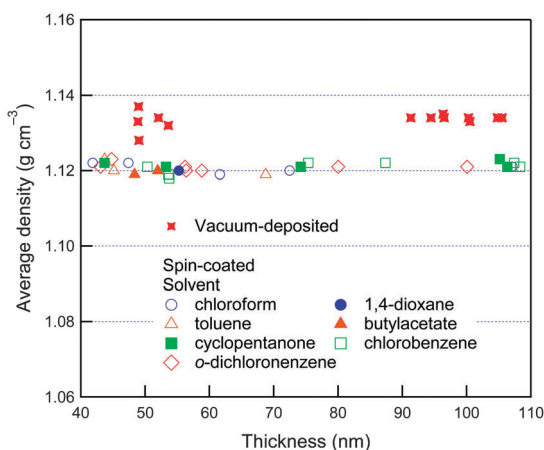

Fig. 5 Densities of spin-coated TPD films fabricated using different solvents, spin speeds, and solution concentrations. The densities of vacuum-deposited films with different thicknesses are also shown for comparison.

This journal is © The Royal Society of Chemistry 2015

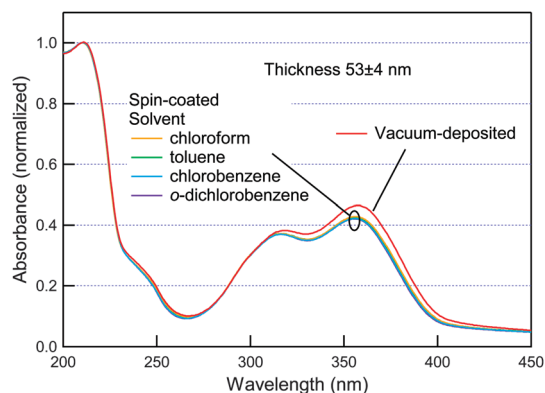J. Mater. Chem. C, 2015, 3, 11178–11191 | 11181

Fig. 6 Normalized absorption spectra of spin-coated TPD films fabricated using four different solvents and a vacuum-deposited TPD film. All films had approximately the same thickness of 53 ± 4 nm: 49.6 nm (chloroform), 51.1 nm (toluene), 53.8 nm (chlorobenzene), 56.3 nm (*o*-dichlorobenzene), and 52.3 nm (vacuum-deposited).

Fig. 7 Changes of the densities of vacuum-deposited (red) and spin-coated (blue) TPD films with a thickness of ∼70 nm during heating–cooling cycles. The temperature during the cycles is also shown (green). The gray dotted horizontal line shows the identical densities of the transition-experienced vacuum-deposited film and the spin-coated film at room temperature.

In addition, we determined the densities of vacuum-deposited and spin-coated films of 4-[*N*-(1-naphthyl)-*N*-phenylamino]-4′-[*N*-(1-naphthyl)-*N*-(4-octylphenyl)amino] biphenyl (α-ONPD, see Fig. 2) to investigate the effect of the alkyl side chain attached to α-NPD for high solubility. As shown in Table 1 (see also Fig. S1(e), ESI† for more details), the difference between the densities of vacuum-deposited and spin-coated α-ONPD films is smaller than that for α-NPD films, though the vacuum-deposited films still have a slightly higher density than that of the spin-coated ones. This is probably because the void is filled by the thin octyl chains. However, this result does not mean that spin-coated films of a material with an alkyl chain have better properties than those without it. If we exclude the volume of the octyl group from V_{vdW} in eqn (1), the K_p values of the vacuum-deposited and spin-coated α-ONPD films are 0.56 and 0.55, respectively. Because the alkyl groups are nonconductive, these are the substantive K_p values of α-ONPD as a semiconducting material.

2.2 Transition temperature

To understand the difference in the density of films fabricated by different methods, we investigated the temperature dependence of film density. Using an ellipsometer with a temperature-control stage, we performed *in situ* ellipsometry measurements and traced the change of the densities of vacuum-deposited and spin-coated films during heating–cooling cycles.

Fig. 7 shows the variations in the density of vacuum-deposited and spin-coated TPD films with a thickness of ∼70 nm with temperature. We heated each sample at a rate of 3 °C min^{-1} up to 100 °C, which is much higher than the glass transition temperature of 60 °C of the TPD powder,[17] kept the sample at 100 °C for 30 min, and then naturally cooled it to 30 °C. We repeated this cycle twice for each sample to clarify what occurs in the first cycle. When the vacuum-deposited film was first heated (0–15 min in the bottom axis), the density gradually decreased because of the thermal expansion of the film. Then, at a temperature of 72 °C (around 19 min), the density abruptly decreased. This is caused by the transition of the film induced
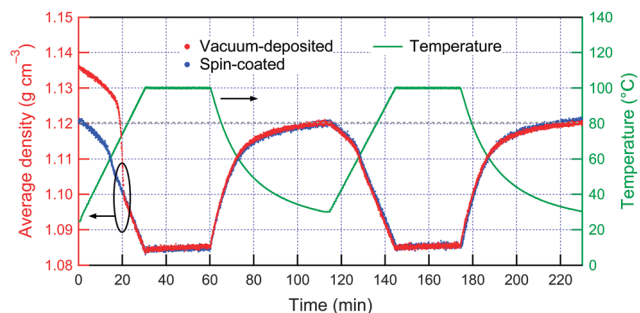
by heating. After the temperature was kept at 100 °C (30–60 min), the density gradually increased during the cooling process (60–115 min) because of the thermal shrinkage of the film. In the second cycle, the film repeated the thermal expansion and shrinkage of the first cycle, except that the abrupt decrease of density was not observed in the heating process. We note here that the film density did not completely recover after cooling in the first cycle; that is, there was a significant difference between the film densities before and after the first cycle, whereas the densities before and after the second cycle were the same. Although similar changes in the density of vacuum-deposited organic films have been reported,[11,13] here we emphasize the quantitative difference between the absolute densities before and after the first cycle and the identity before and after the second cycle.

The density of spin-coated TPD films showed markedly different behaviours during heating–cooling cycles, which has not been reported before. In the first heating process, an abrupt decrease in density was not observed, though the slope of the decrease did change at 55 °C (12 min), which is the glass transition of the spin-coated film. The important facts that we should note are that (1) the density of the spin-coated film completely recovered after the first and second cycles, though the original density of the film was lower than that of the vacuum-deposited one, (2) the densities of the spin-coated films before and after each cycle are quantitatively identical to that of the "transition-experienced" vacuum-deposited film at room temperature following its first heating cycle, and (3) the transition temperature of the spin-coated film in the first heating cycle (55 °C) is much lower than that of the vacuum-deposited film (72 °C). Qualitatively similar results were also observed using other materials (see Fig. S7, ESI†). In addition, we confirmed that the density of a spin-coated film after heating did not come close to that of a vacuum-deposited film, even when the film was cooled very slowly over 4 h (see Fig. S8(a), ESI†).

To clearly demonstrate the differences in the transition temperature and thermal stability of TPD films fabricated by different methods, we show the thickness change $(d - d_0)/d_0$ of the vacuum-deposited film in Fig. 8(a), where d is the thickness

11182 | *J. Mater. Chem. C*, 2015, **3**, 11178–11191

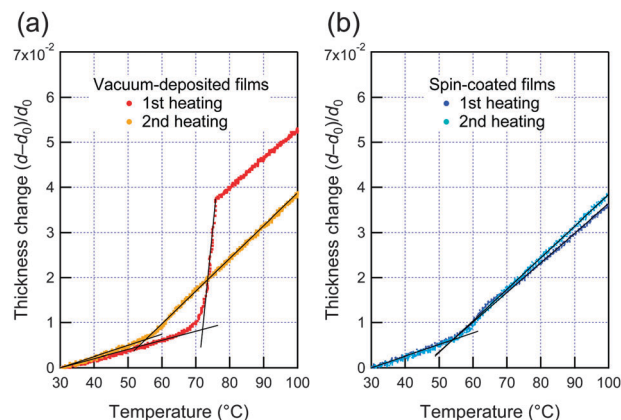This journal is © The Royal Society of Chemistry 2015

Fig. 8 Thickness changes of (a) vacuum-deposited and (b) spin-coated TPD films during the first and second heating processes. The slopes are the thermal expansion coefficients, and the cross points of the slope lines (black lines) show the transition temperatures.

Table 2 Transition temperatures of the powder, vacuum-deposited films, and spin-coated films of various OLED materials[a]

Material	TPD	α-NPD	2-TNATA	TPT1	TSBF
Powder[b]	60	96	110	144	231
Vacuum-deposited film	72	108	124	151	227
Spin-coated film	55	86	101	137	217

[a] The unit of all temperatures is °C. [b] The glass transition temperatures of all powders are cited from ref. 17 and 31–34.

of the film during the first and second heating processes, and d_0 is the thickness before each heating process. The slopes correspond to the thermal expansion coefficients of the films. In the first heating, the thickness increased linearly up to around 72 °C, and then it suddenly jumped in a discontinuous manner, where a drastic change from a stable solid to a super-cooled liquid occurred in the film.[13] This temperature is higher than the glass transition temperature of the TPD powder (60 °C), meaning that the molecular aggregation state in the vacuum-deposited films is more stable than that in the bulk of the powder. However, once the film experienced the transition in the first cycle, the thickness showed different behavior in the second cycle; the thickness changed continuously, and the thermal expansion coefficient changed at 56 °C. This is the glass transition temperature of the vacuum-deposited film that had already experienced the transition once in the first heating cycle, and it is lower than the glass transition temperature of the TPD powder. In contrast, the thickness of the spin-coated TPD film changed continuously in a similar manner in both the first and second heating cycles, as shown in Fig. 8(b). The thermal expansion coefficient changed at 55 °C in both the first and second heating cycles, which is nearly the same as the glass transition temperature of the transition-experienced vacuum-deposited film in its second heating cycle. These results clearly show the differences in the transition temperatures of the vacuum-deposited and spin-coated films, and demonstrate that the thermal stability of the spin-coated film is lower than that of the vacuum-deposited one. We emphasize that the thicknesses of the spin-coated film in the first and second heating cycles showed a very similar trend to that of the transition-experienced vacuum-deposited film in its second heating cycle. This result suggests the macroscopic identity of the spin-coated and transition-experienced vacuum-deposited films. The vacuum-deposited and spin-coated films of other materials also qualitatively showed the same results (see Fig. S9, ESI†). Table 2 summarizes the differences in the transition temperatures of powders, vacuum-deposited films, and spin-coated films of various OLED materials.

The UV-vis absorption spectra of the solid films also support the macroscopic identity of the spin-coated and transition-experienced vacuum-deposited films. In Fig. 9, the absorption spectra of three TPD films with approximately the same thickness of 48 ± 2 nm are shown without normalization; the spectra are of an as-prepared vacuum-deposited film, a transition-experienced vacuum-deposited film, and a spin-coated film. We can clearly see the difference between the spectra of the vacuum-deposited and spin-coated films, as already discussed, and the identity of the spectra of the spin-coated film and the transition-experienced vacuum-deposited one. Similar results were also observed using other materials (see Fig. S10, ESI†).

The lower transition temperatures of the spin-coated films than those of the vacuum-deposited ones mean that their thermal stabilities are lower, showing a disadvantage of small-molecule spin-coated films compared to vacuum-deposited ones. Furthermore, the identical densities, transition temperatures, and absorption spectra of the transition-experienced vacuum-deposited films and spin-coated ones indicate that the small-molecule spin-coated films are macroscopically equivalent to the "deteriorated" vacuum-deposited films that have experienced a transition during a heating cycle. Although it seems that the change in the density of the spin-coated films during the heating–cooling cycles is reversible, it does not mean that they possess high thermal stability. The change in spin-coated films seems to be reversible only when the film is a single layer; in a multilayer structure, the irreversible mixing of materials at interfaces cannot be avoided at temperatures exceeding the transition temperature.[35] Such interfacial mixing at high temperature is currently being investigated by ellipsometry and will be reported in a future study.
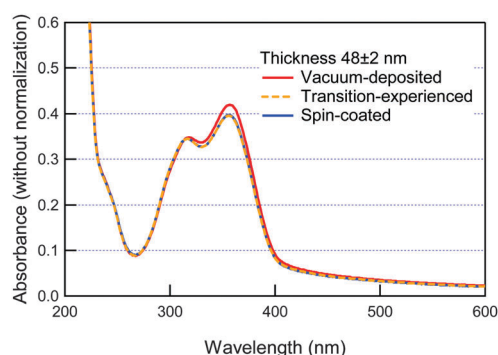

Fig. 9 Absorption spectra without normalization of the as-prepared and transition-experienced vacuum-deposited TPD films, and a spin-coated TPD film. The original thicknesses of the vacuum-deposited and spin-coated films were approximately the same (47.0 and 49.1 nm, respectively).

This journal is © The Royal Society of Chemistry 2015

J. Mater. Chem. C, 2015, 3, 11178–11191 | 11183

2.3 Molecular orientation

Another important difference between vacuum-deposited and spin-coated films is their molecular orientation. Recently, we have found that horizontal molecular orientation generally occurs depending on the molecular shape even in small-molecule vacuum-deposited OLED films and have demonstrated its considerable effects on both the electrical and optical characteristics of films and devices.[2] Thus, clarification of the difference in molecular orientation in films formed by vacuum deposition and spin coating is very important to explain the differences in device performance. To investigate the general differences between the molecular orientations in vacuum-deposited and spin-coated films of small-molecule OLED materials, we selected four materials shown in Fig. 2: 4,4′,4″-tris[2-naphthyl(phenyl)amino]triphenylamine (2-TNATA), $N^4,N^{4'}$-(biphenyl-4,4′-diyl)bis($N^4,N^{4'},N^{4'}$-triphenylbiphenyl-4,4′-diamine) (TPT1), 2,7-bis(9,9-spirobifluoren-2-yl)-9,9-spirobifluorene (TSBF), 4,4′-bis[4-(diphenylamino)styryl]biphenyl (BDAVBi), which are materials known to prefer horizontal molecular orientation and that exhibit large birefringence.[23,33,36] The absolute densities of their vacuum-deposited and spin-coated films determined by UV-vis absorption measurements of solutions and ellipsometry analysis are summarized in Table 1 (also see Fig. S1(f)–(i), ESI† for more details). Similar to the cases described above, the densities of the vacuum-deposited films were higher than those of the spin-coated ones. We also confirmed that the densities of spin-coated films of 2-TNATA and TPT1 were constant when the film thickness was >30 nm (see Fig. S3(d) and (e), ESI†).

Fig. 10 shows the changes in the density of vacuum-deposited and spin-coated 2-TNATA films during heating–cooling cycles, which were determined by *in situ* ellipsometry using an anisotropic optical model. The changes in the density were qualitatively the same as those of TPD and α-NPD films. The density of the vacuum-deposited film abruptly decreased during the first heating cycle, and it did not completely recover even after cooling. In contrast, the densities of the spin-coated films before and after a heating cycle were the same, and identical to the density of the transition-experienced vacuum-deposited film.
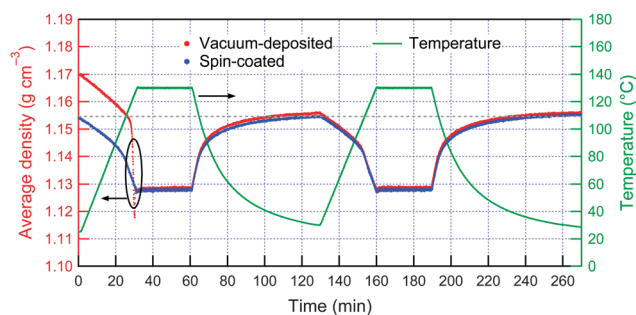
Furthermore, the transition temperature of the vacuum-deposited films in the first heating cycle was higher than that of the spin-coated film. We also observed similar behaviour for TPT1 and TSBF (see Table 2 and Fig. S7 and S9, ESI†).

The analysis of the ellipsometry data clearly revealed the difference between the molecular orientations of vacuum-deposited and spin-coated 2-TNATA films with a thickness of ~100 nm, as shown in Fig. 11(a) and (b), respectively. For the vacuum-deposited film, the refractive index and the extinction coefficient in the horizontal direction (n_o and k_o, respectively) were much larger than those in the vertical direction (n_e and k_e, respectively), meaning that the molecules are significantly oriented in the horizontal direction.[2] In contrast, the optical constants of the spin-coated film were isotropic, meaning that molecules in the spin-coated film are randomly oriented. Interestingly, both the spin-coated and transition-experienced vacuum-deposited films exhibited random molecular orientations, as shown in Fig. 11(b) and (c), respectively. The molecular orientation in the spin-coated film is random as that in the vacuum-deposited film that had experienced a transition induced by the heating process. Although the change of the orientation from horizontal to random induced by heating vacuum-deposited films has long been known,[37] the analogy of spin-coated and transition-experienced films observed here has never been discussed. The absorption spectra of solid films on fused silica substrates in Fig. 12 further confirm the identical random orientation of the spin-coated film and the transition-experienced vacuum-deposited one, because a large difference in orientation is reflected in the absorbance of the absorption peaks.[38,39] These trends of anisotropy and absorption spectra were also qualitatively common to TPT1, TSBF and BDAVBi (see Fig. S10 and S11, ESI†).

In addition, we found that the anisotropy of spin-coated 2-TNATA films is not strongly affected by the experimental conditions of spin speed and solution concentration, as shown
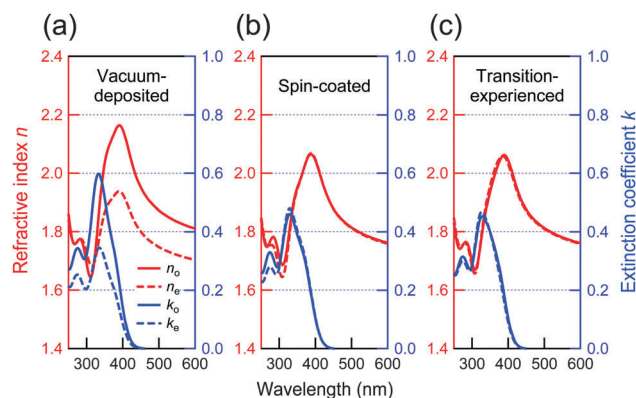
Fig. 10 Changes of the densities of vacuum-deposited (red) and spin-coated (blue) 2-TNATA films with a thickness of ~100 nm during heating–cooling cycles. The temperature during the cycles is also shown (green). The gray dotted horizontal line shows the identical density of the transition-experienced vacuum-deposited film and the spin-coated film at room temperature.

Fig. 11 Anisotropic optical constants of the (a) as-prepared vacuum-deposited film, (b) spin-coated film, and (c) transition-experienced vacuum-deposited film of 2-TNATA with a thickness of ~100 nm. The red solid and broken lines show the refractive indices in the horizontal and vertical directions (n_o and n_e), respectively, and the blue solid and broken lines show the extinction coefficients in the horizontal and vertical directions (k_o and k_e), respectively.

11184 | *J. Mater. Chem. C*, 2015, **3**, 11178–11191

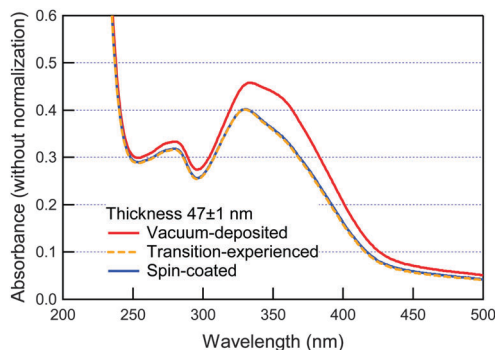This journal is © The Royal Society of Chemistry 2015

Fig. 12 Absorption spectra without normalization of the as-prepared and transition-experienced vacuum-deposited 2-TNATA films, and a spin-coated 2-TNATA film. The original thicknesses of the as-prepared vacuum-deposited and spin-coated films were approximately the same (46.5 and 47.8 nm, respectively).
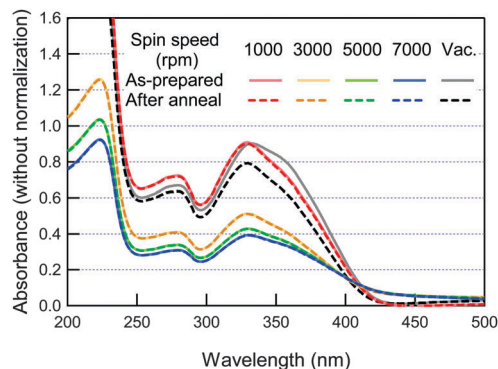

Fig. 14 Absorption spectra without normalization of the as-prepared and transition-experienced spin-coated 2-TNATA films fabricated with a solution concentration of 15 mg ml^{-1} and different spin speeds. Absorption spectra of the as-prepared and transition-experienced vacuum-deposited 2-TNATA film with a thickness of ~100 nm are also shown.

in Fig. 13. Because ellipsometry analysis becomes relatively insensitive to anisotropy in thin films with a thickness of <100 nm, here we used a simple optical model for the analysis of the transparent spectral region: the Cauchy model with the additional anisotropic parameter of birefringence Δn, which is a constant representing the difference between n_o and n_e. Because Δn is directly related to the anisotropy of the molecular polarizability in a film,[2] the more significant the horizontal orientation of 2-TNATA molecules is, the larger the Δn becomes. For all experimental conditions investigated (spin speed of 1000–7000 rpm and solution concentration of 10–20 mg ml^{-1}), the birefringences of the spin-coated films were not more than 0.025, which is much lower than that of the vacuum-deposited film (0.107). This result shows that the molecular orientation in the spin-coated films is nearly random over a wide range of spin-coating conditions, and the degree of the horizontal molecular orientation in the spin-coated films is much lower than that in the vacuum-deposited ones. This conclusion is also strongly supported by the absorption spectra of the as-prepared and transition-experienced spin-coated films shown in Fig. 14. In contrast to the considerable decrease of absorbance of a vacuum-deposited 2-TNATA film by a transition, the absorbance of all spin-coated 2-TNATA films fabricated with a solution concentration of 15 mg ml^{-1} and spin speeds of 1000–7000 rpm did not significantly change even after they experienced a transition

induced by heating. Assuming that molecular orientations in all of these films become random *via* the transition, this result means that molecular orientation of spin-coated films is originally almost random independently of the spin speed. Similar results were also found for spin-coated TPT1 films (see Fig. S12 and S13, ESI†).

Fig. 15 shows how the molecular orientation in a vacuum-deposited film changed during the heating–cooling cycles, which was determined from the *in situ* analysis of the anisotropy in the extinction coefficients of a vacuum-deposited 2-TNATA film with a thickness of ~100 nm. The change of the anisotropy of the extinction coefficients $\Delta k = k_o - k_e$ at 332 nm (the wavelength of the highest peak) is shown. Once the original vacuum-deposited film with a large Δk of 0.23 experienced a transition at 124 °C during its first heating cycle, the anisotropy became very small and did not recover during the first and second cooling cycles. We also confirmed that the molecular orientation of 2-TNATA did not recover even when we cooled the film very slowly over 4 h (see Fig. S8(b), ESI†). In addition, we further investigated the anisotropy and absorption spectra of 2-TNATA films fabricated using three other solvents having different boiling points (Fig. S14 and S15, ESI†). There was no significant dependence of molecular orientation and absorption on solvent under the experimental conditions in this study.
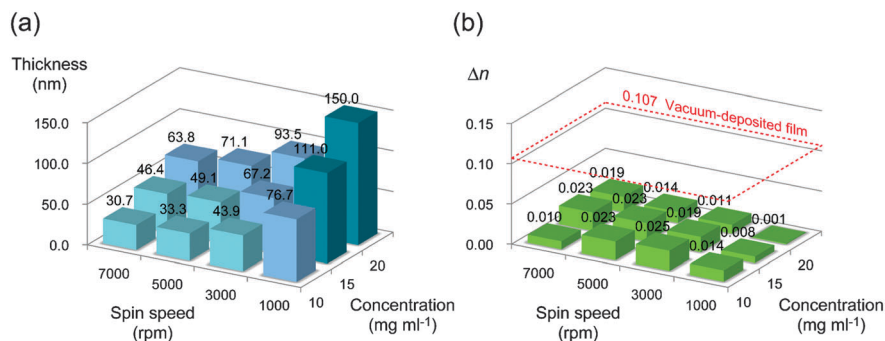

Fig. 13 (a) Thicknesses and (b) birefringences of spin-coated 2-TNATA films fabricated using chloroform as the solvent with different spin speeds and solution concentrations. The birefringence of the vacuum-deposited 2-TNATA film is also shown as a red dotted line.
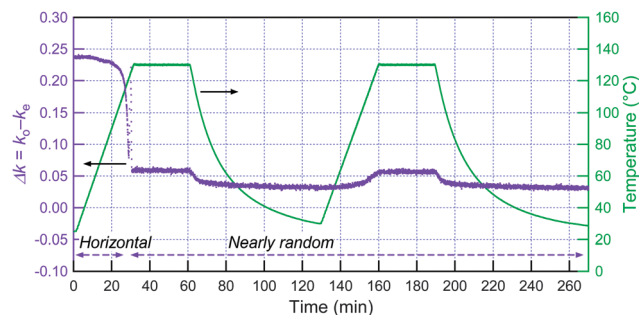
This journal is © The Royal Society of Chemistry 2015

J. Mater. Chem. C, 2015, **3**, 11178–11191 | 11185

Fig. 15 Change of the anisotropy of extinction coefficients $\Delta k = k_o - k_e$ at 332 nm of vacuum-deposited 2-TNATA films with a thickness of $\sim$100 nm during heating–cooling cycles. The temperature during the cycles is also shown (green).

Fig. 16 Thickness changes of vacuum-deposited 2-TNATA films fabricated at different deposition rates of 0.2, 2, and 20 Å s^{-1} during a heating–cooling cycle. To compare the densities of the as-prepared films, the thicknesses at 40 °C after cooling d_0' are used as the standards for normalization.

Our results show the irreversibility of the density and molecular orientation of vacuum-deposited films during the first heating cycle, and the macroscopic identity of transition-experienced films and spin-coated films of OLED materials having large anisotropy of molecular shape.

The nearly random orientation of small-molecule spin-coated films is a disadvantage when compared to vacuum-deposited films because horizontal molecular orientation has positive effects on both the electrical and optical characteristics of films and devices. Our results show that it is not easy to achieve a high degree of horizontal orientation by a simple spin-coating process using common amorphous materials. Therefore, it is difficult to enhance charge transport in small-molecule spin-coated films or the outcoupling efficiency of OLEDs containing them by actively utilizing the horizontal molecular orientation of charge transport materials or emitting materials, respectively.[2] However, we should also focus on the advantages of small-molecule spin-coated films: low cost and ease of fabricating large-area devices. If we can solve the difficulty in realizing the high degree of the horizontal orientation in small-molecule solution-processed films, the OLED devices using them will have many advantages.

2.4 Origin of the differences between small-molecule vacuum-deposited and spin-coated films

To overcome the disadvantages of small-molecule spin-coated films in the future, it is important to understand the origin of their differences from vacuum-deposited films. The distinct similarity of spin-coated and transition-experienced films demonstrated above provides a clue to it.

In vacuum-deposited films, each molecule on the surface is highly mobile without being strongly restricted by other molecules in its diffusion. The molecules on the surface have a time in the order of seconds to sample different ways of molecular packing and find a stable higher-order structure before being overlaid by successive molecules. (If we roughly assume that the effective diameter of a small molecule is $\sim$1 nm, the deposition rate of 2 Å s^{-1} means that each molecule has $\sim$5 s for surface diffusion.) This surface diffusion of highly mobile molecules contributes to the high density and stability of vacuum-deposited amorphous organic films.[12]
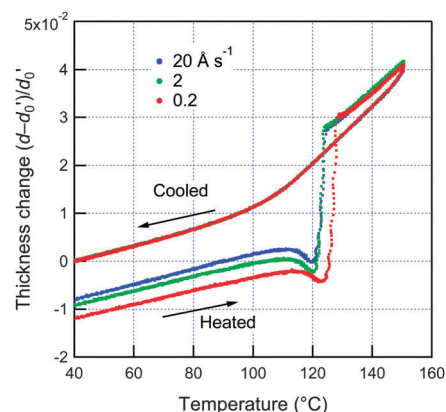
To demonstrate this effect of surface diffusion, we investigated the differences in density and thermal stability of vacuum-deposited 2-TNATA films when we changed the deposition rate. Fig. 16 shows the thickness changes $(d - d_0')/d_0'$ of 2-TNATA films fabricated at different deposition rates of 0.2, 2, and 20 Å s^{-1} when they were heated at a rate of 3 °C min^{-1} up to 150 °C and then naturally cooled down, where d_0' is the thickness of the film at 40 °C after cooling. Here, we assumed that the densities of these three films become the same after the transition by heating, and used the thicknesses of d_0' as the standards for normalization. This assumption is reasonable because the state of supercooled liquids after the transition does not keep the higher-order structure before the transition at all. The film fabricated at 0.2 Å s^{-1} showed the maximum difference between the thickness changes before and after the heating–cooling cycle, demonstrating that the as-prepared film fabricated at a low deposition rate of 0.2 Å s^{-1} has a higher density than the other as-prepared ones. Furthermore, Fig. 16 shows that the film fabricated at 0.2 Å s^{-1} has a higher transition temperature than the others, meaning its higher thermal stability. Similar trends were also observed for vacuum-deposited TPD and TPT1 films (see Fig. S16, ESI†). These results directly demonstrate that the long time for surface diffusion contributes to high densities and high thermal stabilities of vacuum-deposited films.

In addition, we also found another important fact to understand the mechanism of the molecular orientation; the horizontal molecular orientation in vacuum-deposited films occurs just because horizontally oriented molecules on the surface are fixed by successively overlaying molecules, NOT because the state of horizontal orientation is more thermodynamically stable than that of random and vertical orientations in the bulk of the film. Fig. 17 shows the optical anisotropies of the vacuum-deposited 2-TNATA films fabricated at different deposition rates of 0.2, 2, and 20 Å s^{-1}. Interestingly, the degree of the horizontal orientation is highest in the film fabricated at a high deposition rate of 20 Å s^{-1}, whose density and thermal stability are lowest among the three films. A similar trend was also observed for
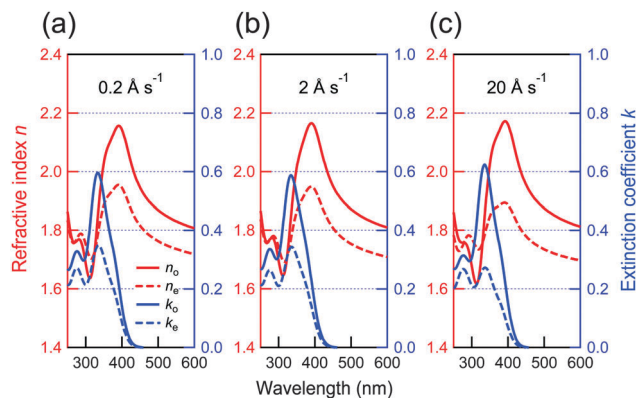
11186 | J. Mater. Chem. C, 2015, 3, 11178–11191

This journal is © The Royal Society of Chemistry 2015

Fig. 17 Anisotropic optical constants of vacuum-deposited 2-TNATA films with a thickness of $\sim$100 nm fabricated at deposition rates of (a) 0.2, (b) 2, and (c) 20 Å s^{-1}. The red solid and broken lines show the refractive indices in the horizontal and vertical directions (n_{o} and n_{e}), respectively, and the blue solid and broken lines show the extinction coefficients in the horizontal and vertical directions (k_{o} and k_{e}), respectively.

vacuum-deposited TPD films, where the film fabricated at 20 Å s^{-1} shows horizontal orientation though the one fabricated at 2 Å s^{-1} shows nearly random orientation (see Fig. S17, ESI†). These results show that the horizontal molecular orientation of these materials is not directly related to the high density or thermal stability of the vacuum-deposited films. Molecules deposited on the surface first adopt horizontal orientation just to minimize the surface energy, but if they can have a longer time for surface diffusion without being overlaid by successively deposited molecules, the molecular orientation changes to random (and further vertical), which is more thermodynamically stable, by the collaborative structural relaxation with other diffusing molecules on the surface.[2,38,40] This mechanism is consistent with the fact that the molecular orientation in amorphous vacuum-deposited films can be controlled from horizontal to random and further vertical by heating the substrate during deposition.[38,40] Thus, the horizontally oriented states are caused by the restriction of the structural relaxation in amorphous solids, and they are metastable states having a local minimum energy with kinetic stability in the energy landscape.[41]

In contrast to vacuum-deposited films, spin-coated and transition-experienced films are formed by a mechanism distinctly different from that of vacuum-deposited ones; many small molecules in the films are simultaneously condensed and solidified. During these processes, molecular motion for structural relaxation is strongly limited by the surrounding molecules. The higher-order structures of spin-coated and transition-experienced films are readily trapped at a state having a local minimum energy in the energy landscape that is less stable than that of vacuum-deposited ones. As a result, films have relatively larger voids, resulting in a lower thermal stability.

At the same time, we should also note that the times for the change from a liquid to a solid are different for spin-coated and transition-experienced films. In the spin-coating process, most of the solvent is vaporized in a short time, at most a few tens of seconds. Conversely, the cooling process of films after transition is very slow; the longest time for cooling in this study was

4 h (see Fig. S8, ESI†). Although these time scales are quite different, the films are macroscopically identical as discussed above. This shows that the time for the formation of the solid films is not the primary factor that causes the differences between vacuum-deposited and spin-coated films, at least when we fabricate films in a realistic time for production (within several hours). This conclusion is consistent with the estimation that it takes more than thousands of years to achieve ordinary glasses with a density as high as that of vacuum-deposited amorphous films.[11]

Because simply lengthening the time for film formation cannot compensate the differences, we have to find another way to realize small-molecule solution-processed films having high thermal stability and a high degree of horizontal molecular orientation. From the above discussion, we can see that one possible strategy is to develop new materials that can adopt a stable higher-order structure even when their molecular motion is strongly restricted by surrounding molecules. We think that the active use of intermolecular interactions[39,42] is a possible way to achieve this in the future, even though it has not yet been explicitly discussed in studies on small-molecule solution-processed OLEDs.

2.5　Polymer film

Although small-molecule spin-coated films currently have the disadvantages of their smaller anisotropy of molecular orientation and lower thermal stability than vacuum-deposited ones, it has been well known for a long time that spin-coated polymer films often tend to form horizontal molecular orientation.[43–46] Furthermore, in general, the larger the molecular weight of a polymer or an oligomer is, the higher its glass transition temperature is.[17,47] Thus, we can expect that the use of spin-coated polymers enables us to avoid the disadvantages of the small anisotropy and lower thermal stability of small-molecule spin-coated films. To demonstrate this, we fabricated a spin-coated film of poly[N,N'-bis(4-butylphenyl)-N,N'-bis(phenyl)-benzidine] (poly-TPD), whose chemical structure is shown in Fig. 2, and analyzed the optical anisotropy and transition temperature of the resulting film. Because the unit structure of poly-TPD is very similar to those of TPD and TPT1, we can roughly regard poly-TPD as a molecule consisting of a large number of TPD units, and TPT1 as a molecule consisting of two TPD units. To investigate the effect of the number of units on the film properties, we compared the optical anisotropies and transition temperatures of spin-coated films of TPD, TPT1 and poly-TPD with a thickness of $\sim$100 nm, which were fabricated using chlorobenzene as the solvent. The optical anisotropies of the films are shown in Fig. 18, revealing that both TPD and TPT1 molecules are almost randomly oriented in the spin-coated films, whereas the chain axis of poly-TPD molecules are horizontally oriented. In Fig. 18(c), the optical anisotropy on the long-wavelength side of the absorption band of poly-TPD can be assigned to the anisotropy of the transition dipole moment along the long axis of the TPD units.[38] The results of in situ ellipsometry analysis during heating processes also confirmed that the transition temperature of the spin-coated
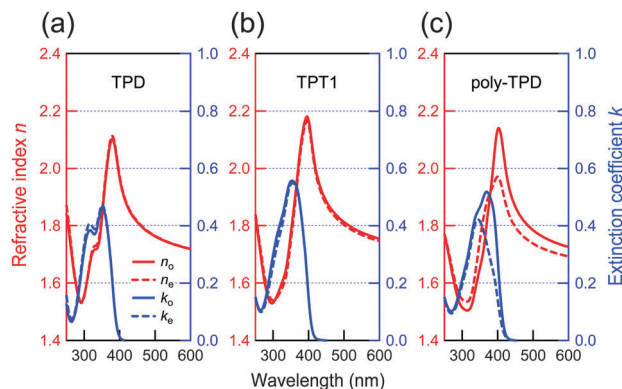
Fig. 18 Anisotropic optical constants of spin-coated films of (a) TPD, (b) TPT1, and (c) poly-TPD with a thickness of ~100 nm. The red solid and broken lines show the refractive indices in the horizontal and vertical directions (n_o and n_e), respectively, and the blue solid and broken lines show the extinction coefficients in the horizontal and vertical directions (k_o and k_e), respectively.
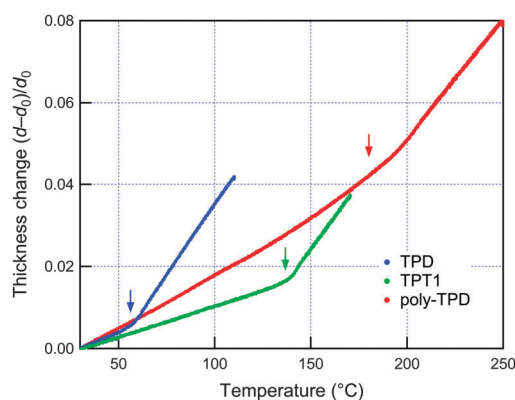

Fig. 19 Thickness changes of spin-coated films of TPD (blue), TPT1 (green), and poly-TPD (red) during heating. The slopes are the thermal expansion coefficients, and the arrows show the glass transition temperatures.

poly-TPD film (180 °C) is much higher than those of the spin-coated TPD and TPT1 films (56 and 136 °C, respectively), as shown in Fig. 19.

The fact that polymer films have larger anisotropy of molecular orientation and higher thermal stability than small-molecule spin-coated films highlights the advantages of polymer films. However, polymer films also have disadvantages, including higher impurity and lower solubility. We should take into account both the advantages and disadvantages of materials when choosing a spin-coating system for OLED fabrication.

3. Conclusions

We systematically compared vacuum-deposited and spin-coated films of the small-molecule OLED materials by ellipsometry, UV-vis absorption, and XRR measurements, and found that the film density, transition temperature, and degree of horizontal molecular orientation of small-molecule spin-coated films are inherently lower than those of the corresponding vacuum-deposited films. In addition, the transition temperature and

molecular orientation of small-molecule spin-coated films of glassy materials are identical to those of the "deteriorated" vacuum-deposited films that had experienced a transition induced by heating. We also confirmed the higher thermal stability and larger anisotropy of molecular orientation of a polymer spin-coated film compared to those of the corresponding small-molecule spin-coated films.

The relative advantages and disadvantages of each type of film at present are summarized as follows.
(i) Small-molecule vacuum-processed films:
 – Advantages: ease of stacking an ideal multilayer structure, high thermal stability, high material purity, and high degree of horizontal molecular orientation
 – Disadvantages: high cost of fabrication processes and difficulty in fabricating large-area devices
(ii) Small-molecule solution-processed films:
 – Advantages: low cost of fabrication processes and ease of fabricating large-area devices
 – Disadvantages: low thermal stability of the film, small anisotropy of molecular orientation, and difficulty in fabricating an ideal multilayer structure
(iii) Polymer solution-processed films:
 – Advantages: low cost of fabrication processes, ease of fabricating large-area devices, high thermal stability, and high degree of horizontal molecular orientation
 – Disadvantages: low material purity, low solubility, and difficulty in fabricating an ideal multilayer structure

Our comprehensive comparisons lead to guidelines to help choose an appropriate process and materials to produce OLED displays or lighting according to the requirement of a specific situation.

Although we have mainly demonstrated the disadvantages of small-molecule spin-coated films in this study, we would finally like to emphasize that our results do not exclude the possibility of overcoming them. One of the purposes of this study is to clarify the future challenges that need to be solved to realize high-performance solution-processed OLEDs using small molecules, which is important for researchers who are trying to solve the problems and improve device performance. We believe that it will be possible to overcome some of the above disadvantages by actively utilizing intermolecular interactions, which have not yet been considered explicitly in relation to solution-processed OLED films.

4. Experimental

4.1 Sample fabrication

TPD, α-NPD, α-ONPD, 2-TNATA, TPT1, TSBF, BDAVBi, and poly-TPD were purchased from Luminescence Technology Corporation. (α-NPD and α-ONPD are sold as "NPB" and "ONPB", respectively.) CBP and Alq$_3$ were purchased from e-Ray Optoelectronics Technology. All of the small-molecule materials were of sublimed grade. Si(100) substrates without a thermally oxidized layer were used for the UV-vis absorption measurements of the dissolved solutions of the films, XRR measurements, and ellipsometry.

11188 | J. Mater. Chem. C, 2015, 3, 11178–11191

This journal is © The Royal Society of Chemistry 2015

Fused silica substrates were used only for the UV-vis measurements of solid films. All vacuum-deposited films were fabricated at a deposition rate of 2 Å s^{-1}, unless noted otherwise, under a vacuum of $<1 \times 10^{-3}$ Pa. Spin-coated films were fabricated under a wide range of experimental conditions, including different solvents, solution concentrations, and rotation speeds, depending on the purpose of each analysis. Chloroform was used as the solvent unless noted otherwise. The spin-coating time was 50 s. After spin-coating, all of the spin-coated films except the TPD ones were baked at 80 °C for 30 min under a nitrogen atmosphere. TPD films were baked at 50 °C for 30 min because they have a low transition temperature.

When comparing the absorption spectra of the vacuum-deposited and spin-coated films without normalization, the spin-coated films were first fabricated and analyzed, and then the vacuum-deposited films were fabricated so that the thickness of the vacuum-deposited films were the same as that of the spin-coated ones. When preparing the transition-experienced films, the as-prepared films were annealed on a hot plate under a nitrogen atmosphere at a temperature much higher than the glass transition temperature of the material and then naturally cooled to room temperature.

All of the experimental conditions used to fabricate films and the resulting thickness of each sample are summarized in Table S1 (ESI†).

4.2 UV-vis absorption measurements of dissolved films

The main procedures used to obtain film densities from UV-vis absorption measurements of dissolved films have been described elsewhere.[18,19] In our case, films were deposited on Si(100) substrates using a metal mask to precisely define the area of the films (20 × 20 mm^2 with an error of ±4 mm^2). This guaranteed a small error of the area of ±1%. From this area and the thickness obtained by ellipsometry analysis, film volumes were determined. The films were dissolved in chloroform or toluene, and the volumes of the solutions were carefully adjusted to 10 ± 0.03 ml. Reference solutions of each material with definite concentrations were also prepared to make calibration lines.

UV-vis absorption spectra were recorded using a spectrophotometer (UV2450, Shimadzu). From the peak absorbance, the concentrations of each dissolved film were determined using the calibration lines, and the densities of the films were estimated. The detailed results of this analysis are presented in Fig. S1 (ESI†).

4.3 XRR measurements

The films for XRR measurements were deposited on Si(100) substrates. Because the densities of organic materials are usually lower than those of inorganic substrates such as a Si substrate, the critical angles for the organic films appear at a smaller angle than that for the Si substrate.[21,22] In this case, the critical angle for an organic film in the XRR patterns often becomes blurred, especially when the organic film is thin. Thus, to make the critical angle for organic films clearly apparent, films having a large thickness of ~300 nm were fabricated. Although it is possible to analyze the fringing patterns in the larger-angle region of XRR patterns of thin films, this was not done here because the analysis of the fringing patterns of organic films is easily affected not only by density but also surface roughness, which makes it difficult to obtain a unique solution of clear density results.

The XRR patterns of the samples were measured using an X-ray diffractometer (SmartLab, Rigaku) under Cu Kα (λ = 1.54178 Å) radiation at 45 kV and 200 mA. The beam divergence angle was 0.04°, and the widths of the divergence, scattering and receiving slits were 0.1, 0.3 and 0.4 mm, respectively. The incident angles were scanned from 0° to 0.5° in steps of 0.002° at a scan rate of 0.2° min^{-1}. Considering the differences between the sample area and the footprint area of the X-ray with very small grazing incident angles, a correction of the measured patterns was performed. The fitting analysis was performed using GlobalFit software (Rigaku). We estimated the error of the absolute densities at the sample surface as ±0.04 g cm^{-1} or less. The detailed results are presented in Fig. S2 (ESI†).

4.4 Ellipsometry analysis

All sample films for ellipsometry analysis were fabricated on Si(100) substrates, whose definite optical constants minimize the error of the results. This choice of substrate is very important because the errors of the optical constants of the underlying substrate affect the results of the analysis of the overlaying organic film and often lead to an incorrect result, especially when analyzing the optical anisotropy of a very thin film. (For example, the use of a glass or fused silica substrate to analyze the anisotropy of very thin films makes the reliability of the results very low, because their transparency causes unwanted back-side reflection and their optical constants depend on the fabrication process.)

For the analysis of density and anisotropy, variable angle spectroscopic ellipsometry (VASE) measurements were performed using a fast spectroscopic ellipsometer (M-2000U, J. A. Woollam) at seven angles of incident light from 45° to 75° in steps of 5°. At each angle, experimental ellipsometric parameters Ψ and Δ were simultaneously obtained in steps of 1.6 nm throughout the spectral region from 245 to 1000 nm.

For the *in situ* measurement during the heating–cooling cycles, we used a temperature-control stage (J. A. Woollam), which was attached to the ellipsometer. The stage was covered by a metallic box with optical windows to avoid exposure to air, and it was kept under a nitrogen atmosphere during the cycles. The angle of incident light was fixed at 70°, and the ellipsometry parameters were monitored in time steps of ~6 s and spectral steps of 1.6 nm from 245 to 1000 nm. The sample films were heated at a constant rate of 3 °C min^{-1} up to a temperature much higher than the transition temperature (the temperatures used for each sample are listed in Table S1, ESI†). After the high temperature was maintained for 30 min, the sample films were naturally cooled to ~30 °C. This heating–cooling cycle was repeated twice.

The Cauchy model was used to analyze the relative densities of the films of TPD, α-NPD, CBP, and Alq$_3$, because their birefringences in the long-wavelength transparent spectral region are not large. For these films, we analyzed the transparent spectral

This journal is © The Royal Society of Chemistry 2015

J. Mater. Chem. C, 2015, **3**, 11178–11191 | **11189**

region of 600–1000 nm, which is apart from the absorption bands of the four materials. After the fitting analysis, we estimated the relative densities of the films using the Lorentz–Lorenz equation,[48]

$$\frac{n^2 - 1}{n^2 + 2} = \frac{4\pi}{3} \frac{N_A \alpha}{M} \rho \propto \rho, \qquad (2)$$

where n is the refractive index, and α is molecular polarizability. We used the refractive indices at 600 nm for the estimations. Because it is difficult to know the precise values for the molecular polarizabilities of each material, we can only estimate the relative densities of the films of materials based on the proportional relation in eqn (2).

In the analysis of the anisotropy of TPD, 2-TNATA, TPT1, TSBF, BDAVBi, and poly-TPD films with a thickness of ~ 100 nm (Fig. 11, 17 and 18), we used the general oscillator model, the details of which are described in ref. 24. When estimating the relative densities of these anisotropic films, we calculated the isotropic refractive index n_{iso} using the following equation[48] and replaced n in eqn (2) with n_{iso},

$$n_{iso} = \sqrt{\frac{2n_o^2 + n_e^2}{3}}. \qquad (3)$$

In the *in situ* analysis of these anisotropic films during the heating–cooling cycles (Fig. 10, 15, and 16), we fixed the positions (peak energies) and widths of the oscillator bands in the general oscillator model based on the results of the VASE analysis of the vacuum-deposited films before heating, because it is necessary to decrease the number of fitting parameters to obtain reliable unique results for an *in situ* analysis performed with only a single angle of incident light. In the *in situ* analysis, the temperature dependence of the optical constants of the Si substrate was also considered.

When analyzing thin spin-coated films with a thickness of <100 nm using the anisotropic optical model, we should note that the VASE analysis becomes relatively insensitive to anisotropy as the films become thinner. This insensitivity often leads to an unreliable solution of the general oscillator model. In particular, the reliability of the anisotropy of extinction coefficients k_o and k_e becomes low with decreasing thickness. Thus, when we investigated the dependence of optical anisotropy on the experimental conditions of spin speed and solution concentration (Fig. 13), we analyzed the transparent spectral region only (600–1000 nm) and used the Cauchy model with an additional anisotropic parameter of birefringence Δn, which is a constant representing the difference between n_o and n_e. This optical model with only four fitting parameters (two Cauchy parameters, Δn, and thickness) is sufficiently simple to guarantee the uniqueness of solutions even when we analyze thin films with a thickness of several tens of nanometers.

Acknowledgements

Notes and references

1 C. W. Tang and S. A. VanSlyke, *Appl. Phys. Lett.*, 1987, **51**, 913.
2 D. Yokoyama, *J. Mater. Chem.*, 2011, **21**, 19187.
3 L. Duan, L. Hou, T.-W. Lee, J. Qiao, D. Zhang, G. Dong, L. Wang and Y. Qiu, *J. Mater. Chem.*, 2010, **20**, 6392.
4 T.-W. Lee, T. Noh, H.-W. Shin, O. Kwon, J.-J. Park, B.-K. Choi, M.-S. Kim, D. W. Shin and Y.-R. Kim, *Adv. Funct. Mater.*, 2009, **19**, 1625.
5 D. Wang, Z. Wu, X. Zhang, B. Jiao, S. Liang, D. Wang, R. He and X. Hou, *Org. Electron.*, 2010, **11**, 641.
6 G. Mao, Z. Wu, Q. He, B. Jiao, G. Xu, X. Hou, Z. Chen and Q. Gong, *Appl. Surf. Sci.*, 2011, **257**, 7394.
7 S. Feng, L. Duan, L. Hou, J. Qiao, D. Zhang, G. Dong, L. Wang and Y. Qiu, *J. Phys. Chem. C*, 2011, **115**, 14278.
8 X. Xing, L. Zhong, L. Zhang, Z. Chen, B. Qu, E. Chen, L. Xiao and Q. Gong, *J. Phys. Chem. C*, 2013, **117**, 25405.
9 S. Prakash, M. Sims, I. Wyrsta, I. D. Parker, D. Kondakov and W. Gao, *SID Symp. Dig. Tech. Pap.*, 2013, **44**, 678.
10 S. F. Swallen, K. L. Kearns, M. K. Mapes, Y. S. Kim, R. J. McMahon, M. D. Ediger, T. Wu, L. Yu and S. Satija, *Science*, 2007, **315**, 353.
11 K. L. Kearns, S. F. Swallen, M. D. Ediger, T. Wu, Y. Sun and L. Yu, *J. Phys. Chem. B*, 2008, **112**, 4934.
12 L. Zhu, C. W. Brian, S. F. Swallen, P. T. Straus, M. D. Ediger and L. Yu, *Phys. Rev. Lett.*, 2011, **106**, 256103.
13 S. S. Dalal and M. D. Ediger, *J. Phys. Chem. Lett.*, 2012, **3**, 1229.
14 S. S. Dalal, Z. Fakhraai and M. D. Ediger, *J. Phys. Chem. B*, 2013, **117**, 15415.
15 K. Ishii, H. Nakayama and R. Moriyama, *J. Phys. Chem. B*, 2012, **116**, 935.
16 H. Nakayama, K. Omori, K. Inoue and K. Ishii, *J. Phys. Chem. B*, 2013, **117**, 10311.
17 S. Tokito, H. Tanaka, K. Noda, A. Okada and Y. Taga, *Appl. Phys. Lett.*, 1997, **70**, 1929.
18 H.-F. Xiang, Z.-X. Xu, V. A. L. Roy, C.-M. Che and P. T. Lai, *Rev. Sci. Instrum.*, 2007, **78**, 034104.
19 G. Wei, X. Xiao, S. Wang, K. Sun, K. J. Bergemann, M. E. Thompson and S. R. Forrest, *ACS Nano*, 2012, **6**, 972.
20 *X-ray and Neutron Reflectivity: Principles and Applications*, ed. J. Daillant and A. Gibaud, Springer, Berlin, 2009.
21 M. Tolan, *X-Ray Scattering from Soft-Matter Thin Films*, Springer Tracts in Modern Physics, Springer, Berlin, 1999, vol. 148.
22 H. Dosch, *Critical Phenomena at Surfaces and Interfaces*, Springer Tracts in Modern Physics, Springer, Berlin, 1992, vol. 126.

11190 | *J. Mater. Chem. C*, 2015, **3**, 11178–11191

This journal is © The Royal Society of Chemistry 2015

23 D. Yokoyama, A. Sakaguchi, M. Suzuki and C. Adachi, *Appl. Phys. Lett.*, 2008, **93**, 173302.

24 D. Yokoyama, A. Sakaguchi, M. Suzuki and C. Adachi, *Org. Electron.*, 2009, **10**, 127.

25 Z. Zhang, E. Burkholder and J. Zubieta, *Acta Crystallogr., Sect. C: Cryst. Struct. Commun.*, 2004, **60**, o452.

26 P. J. Low, M. A. J. Paterson, D. S. Yufit, J. A. K. Howard, J. C. Cherryman, D. R. Tackley, R. Brook and B. Brown, *J. Mater. Chem.*, 2005, **15**, 2304.

27 M. Brinkmann, G. Gadret, M. Muccini, C. Taliani, N. Masciocchi and A. Sironi, *J. Am. Chem. Soc.*, 2000, **122**, 5147.

28 G. L. Slonimskii, A. A. Askadskii and A. I Kitaigorodskii, *Polym. Sci. U.S.S.R.*, 1970, **12**, 556.

29 A. Bondi, *J. Phys. Chem.*, 1964, **68**, 441.

30 M. J. Frisch, *et al.*, Gaussian 09, Revision D.01, Gaussian, Inc., Wallingford CT, 2009.

31 M. Aonuma, T. Oyamada, H. Sasabe, T. Miki and C. Adachi, *Appl. Phys. Lett.*, 2007, **90**, 183503.

32 Y. Park, B. Kim, C. Lee, A. Hyun, S. Jang, J.-H. Lee, Y.-S. Gal, T. H. Kim, K.-S. Kim and J. Park, *J. Phys. Chem. C*, 2011, **115**, 4843.

33 H.-W. Lin, C.-L. Lin, H.-H. Chang, Y.-T. Lin, C.-C. Wu, Y.-M. Chen, R.-T. Chen, Y.-Y. Chien and K.-T. Wong, *J. Appl. Phys.*, 2004, **95**, 881.

34 J.-H. Jou, C.-C. Chen, W.-B. Wang, M.-F. Hsu and C.-J. Wang, *Proc. SPIE*, 2008, **7051**, 70510P.

35 A. R. G. Smith, J. L. Ruggles, H. Cavaye, P. E. Shaw, T. A. Darwish, M. James, I. R. Gentle and P. L. Burn, *Adv. Funct. Mater.*, 2011, **21**, 2225.

36 D. Yokoyama, K. Nakayama, T. Otani and J. Kido, *Adv. Mater.*, 2012, **24**, 6368.

37 H.-W. Lin, C.-L. Lin, C.-C. Wu, T.-C. Chao and K.-T. Wong, *Org. Electron.*, 2007, **8**, 189.

38 D. Yokoyama, Y. Setoguchi, A. Sakaguchi, M. Suzuki and C. Adachi, *Adv. Funct. Mater.*, 2010, **20**, 381.

39 D. Yokoyama, H. Sasabe, Y. Furukawa, C. Adachi and J. Kido, *Adv. Funct. Mater.*, 2011, **21**, 1375.

40 D. Yokoyama and C. Adachi, *J. Appl. Phys.*, 2010, **107**, 123512.

41 P. G. Debenedetti and F. H. Stillinger, *Nature*, 2001, **410**, 259.

42 H. Sasabe and J. Kido, *J. Mater. Chem. C*, 2013, **1**, 1699.

43 E. K. Miller, M. D. McGehee, M. Diaz-Garcia, V. Srikant and A. J. Heeger, *Synth. Met.*, 1999, **102**, 1091.

44 M. Tammer and A. P. Monkman, *Adv. Mater.*, 2002, **14**, 210.

45 C. M. Ramsdale and N. C. Greenham, *Adv. Mater.*, 2002, **14**, 212.

46 J. M. Winfield, C. L. Donley and J.-S. Kim, *J. Appl. Phys.*, 2007, **102**, 063505.

47 T. G. Fox Jr. and P. J. Flory, *J. Appl. Phys.*, 1950, **21**, 581.

48 M. F. Vuks, *Opt. Spectrosc.*, 1966, **20**, 361.